35th Annual International Conference of the IEEE EMBS
Osaka, Japan, 3 - 7 July, 2013

Automated Segmentation of the Choroid in Retinal Optical Coherence Tomography Images

Huiqi Lu, *Member, IEEE*, Nattapon Boonarpha, Man Ting Kwong, and Yalin Zheng*, *Member, IEEE*

***Abstract*—The choroid is a tissue layer at the back of the eye, which can be imaged by optical coherence tomography (OCT). Choroidal thickness has been proven to be correlated to several ophthalmic diseases in several studies. In this paper we proposed a novel segmentation technique to address this challenge. This technique firstly automatically segments the inner boundary of the choroid using a two-stage fast active contour model. It secondly allows a real-time human-supervised automated segmentation on the outer boundary of the choroid. Dice similarity coefficient (DSC) was used to evaluate the agreement between manual annotation and our automated measurements on 30 images captured from patients diagnosed with diabetes. The mean DSC value is 92.7% (standard deviation 3.6%) in the range of 85.5% to 98.1%. Results show that this new technique can achieve choroid segmentation with high accuracy.**

I. Introduction

The choroid is a highly pigmented tissue layer between the outer RPE-Bruch's membrane and the inner sclera. It contains a high blood flow rate and low oxygen extraction. The choroid plays an important role in retinal homeostasis including thermoregulation and excess light absorption [1, 2]. Choroidal thickness has been proven correlated to several ophthalmic diseases, such as age related macular degeneration [3-6], glaucoma [7, 8], central serous chorioretinopathy[9, 10] and diabetic eye diseases [11].

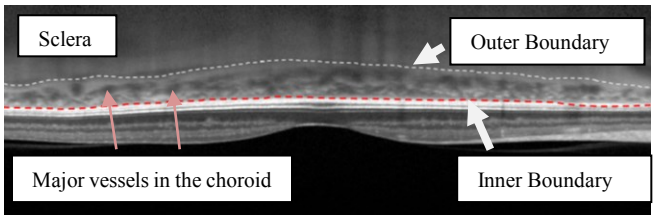

Figure 1. A choroidal image captured by enhanced depth imaging using Heidelberg Spectralis+HRA optical coherent tomography device

In order to study the structure and the cross-sectional morphological details of the choroid, enhanced depth imaging (EDI) on spectral domain optical coherent tomography (OCT) has been widely used. Figure 1 above shows an example of EDI OCT image of the choroid. Outer and inner boundaries are illustrated by white and red dotted lines respectively; the major vessels in the choroid are denoted using red arrows. In this paper, the outer boundary of the choroid was defined as a layer of the supra-choroidal space between choroid and sclera; the inner boundary of the choroid was defined as the outer part of the hyper-reflective line corresponding to the RPE-Bruch's membrane complex.

In the majority of previous studies [4, 5, 10, 12, 13], the boundaries of the choroid were manually delineated for the analysis of its thickness and volume. This is because there is no choroidal segmentation software readily available on the current spectral domain OCT instruments. Manual delineation is slow and is subject to human errors; therefore it is unfeasible for clinical settings and for large scale clinical studies.

Despite the benefits to automate segmentation of the choroid on OCT images in the management of eye disease, it still remains an open question. Due to the limitations on the imaging equipment, as shown in Figure 1, the outer boundary of the choroid has a narrow band or tubular like structure. On the other hand, the inner boundary is relatively easy to segment compare to the outer boundary. Therefore traditional semi- or fully automated segmentation methods might fail in images with average or poor quality. Recent works [14-16] have developed semi- or fully-automated segmentation algorithms for choroid boundaries and choroidal vessel segmentation. Zhang *et al.* [15] used choroidal vasculature to determine the equivalent choroid outer boundary. Hu's semi-automated algorithm [14] can segment the choroid boundaries when poor-quality images were excluded. Kajic's algorithm [16] requires training data to build model for segmentation.

Two segmentation algorithms were proposed in this paper to achieve reliable segmentation of the choroid. The remainder of this paper is organised as follows. Section II described the proposed automated segmentation technique details; section III explained the EDI OCT image dataset used for evaluating the method proposed in section II; section IV is the experimental results and section V is discussion and conclusion.

II. Methods

In this paper, different segmentation algorithms were used to deal with the segmentations of the inner and outer choroidal boundaries respectively so as to achieve high accuracy and efficiency. More specifically, a two-stage variational segmentation strategy (active contour) was used for the inner boundary segmentation, subsequently refined by morphological operations and curve fitting techniques. Our methods then adapted an algorithm from the Live-vessel

This work is supported by the UK National Institute for Health Research's Comprehensive Local Research Networks in Cheshire and Merseyside and the Foundation for Prevention of Blindness, charity No: 10477988.

Huiqi Lu (e-mail: yvonne.lu@liv.ac.uk), Nattapon Boonarpha (e-mail: n.boonarpha@liv.ac.uk), Man Ting Kwong (e-mail: mtkwong@liv.ac.uk) and Yalin Zheng (*corresponding author, phone: +44-151-706-4213; fax: +44-151-706-5802; e-mail: yalin.zheng@liv.ac.uk) are all with the Department of Eye and Vision Science, University of Liverpool, Liverpool, L69 3GA, UK, and the St Paul's Eye Unit, Royal Liverpool University Hospital, Liverpool, L7 8XP, UK.

technique [17] to segment the outer choroidal boundary. The proposed methods were evaluated against the reference standard by manual delineating the choroid performed by an expert.

A. Inner boundary (RPE-Bruch's membrane) segmentation

A fully automated fast global minimization active contour model [18] was adopted to segment the boundary of the RPE-Bruch's membrane complex. This total variational (TV) model is built on Chan and Vese's model [19] which corresponds to the two-phase piecewise constant approximation of Mumford and Shah's model [15]. This algorithm uses dual-projection optimization technique and is chosen for its high speed also global optimality implies that the segmentation is independent of the initialization. The standard algorithm is briefly described below and readers can refer to the original paper for more detail [18]. The energy of the variational model is described as follows:

$$E(u,c_1,c_2,\lambda) = \int_\Omega g(x)|\nabla u|dx + \lambda\int_\Omega ((c_1-f(x))^2-(c_2-f(x))^2)udx \quad (1)$$

Where *f(x)* is the given image, *g* is the edge indicator function and *u* is the characteristic function**.** This model determines the best approximation, in the L^2 space of the image *f(x)* as a set of (non-connected) regions with only two different values, c_1 and c_2. λ is an arbitrary positive parameter that controls the trade-off between the first term and the second term (fidelity term**)**.

For simplicity, we denote:

$$TV_g(u) = \int_\Omega g(x)|\nabla u|dx \quad (2)$$

$$r(x,c_1,c_2) = (c_1-f(x))^2-(c_2-f(x))^2 \quad (3)$$

The dual formulation of the TV-Norm is then minimized by introducing auxiliary variables *v* as follows:

$$\min_{u,v}\{E_2(u,v,c_1,c_2,\lambda,\alpha,\theta) = TV_g(u) + \frac{1}{2\theta}\|u-v\|_{L^2}^2 + \lambda\int_\Omega r(x,c_1,c_2)udx\} \quad (4)$$

Where the parameter *v* is an exact penalty function, α is chosen large enough compared to λ and θ>0 is chosen to be small.

Since functional E_2 is convex, its minimizer can be computed by minimizing E_2, with respect to *u* and *v* separately, and to iterate until convergence [20].

More specifically, the following minimization problems were considered.

(1) When *v* being fixed, we search for *u* as a solution of:

$$\min_u\{TV_g(u) + \frac{1}{2\theta}\|u-v\|_{L^2}^2\} \quad (5)$$

The solution of above is given by:

$$u = v - \theta divp \quad (6)$$

Where *p* is given by:

$$g(x)\nabla(\theta divp - v) - |\nabla(\theta divp - v)|p = 0 \quad (7)$$

The equation (7) can be solved by a fixed point method, in which $p_0 = 0$ and

$$p_{n+1} = \frac{g(x)(p_n + \delta t\nabla(div(p_n) - \frac{v}{\theta}))}{g(x) + \delta t\left|\nabla(div(p_n) - \frac{v}{\theta})\right|} \quad (8)$$

(2) When *u* being fixed, we search for *v* as a solution of:

$$\min_v\{\frac{1}{2\theta}\|u-v\|_{L^2}^2 + \int_\Omega \lambda r\,(x,c_1,c_2)v + \alpha v(v)dx\} \quad (9)$$

The solution of *v* when *u* is fixed is given by:

$$v = \min\{\max\{\,u(x) - \theta\lambda r(x,c_1,c_2),0\},1\} \quad (10)$$

Due to the structural complexity of retinal OCT images, it is not sufficient to segment the RPE-Bruch's complex from the image. A two-stage segmentation strategy was inspired based on the recent work on hierarchical multiphase segmentation models [21, 22]. More specifically, after the first stage, the regions with higher mean intensity are chosen for the segmentation in the second stage. Then the regions with higher mean intensity after the second stage segmentation are chosen for further analysis.

The results of the segmentation after using the above program were refined by morphological operations and curve fitting techniques. The "opening" morphological operations were used to remove small structures which were not part of the high reflectivity band belonging to the RPE-Bruch's complex. After the morphological operation, regions with maximal major axis of >400 pixels are determined and their top boundaries are used to achieve the final segmentation by using a 6-order curve fitting.

B. Outer boundary (sclera-choroid interface) segmentation

For the segmentation of the outer boundary (sclera-choroid interface) of the choroid, an optimized human-interactive automated technique was developed by adapting from the Live-vessel technique [17]. This interactive technique provides the accuracy of a manual segmentation with the speed of an automated segmentation. By putting as few as three seed points on the image boundary, the automated segmentation tool can allocate the optimized boundary. Adding more seed points may give a more precise segmentation. The path can automatically trace along the choroid outer boundary. It is updated in real-time when the user drags the mouse across the screen. The proposed segmentation is achieved by minimizing an energy function model using a dynamic programming technique.

Equation (11) below is the energy to travel between two points, p and q, where $p=(x_1, y_1, r_1)$ and $q=(x_2, y_2, r_2)$. This function calculates a smooth path between point *p* and *q*.

$$E(p,q) = w_1E_v(q) + w_2E_d(p,q) + w_3E_e(q) + w_4E_s(p,q) \quad (11)$$

Where w_i is the weighting parameter *E* represents the energy. In this work, each individual energy term *E* was

normalized to the range of [0, 1] and the weighting parameters were determined empirically.

The first energy term, E_v, examines the grayscale curvature and determines if the pixel lies within a vessel-like tubular structure as described by Frangi *et al* [23]. The eigenvalues $|\lambda_1| \le |\lambda_2|$ of the Hessian matrix of a Gaussian smoothed image are used to calculate the "vesselness" as follows:

$$E_v(q) = \begin{cases} 1 & \lambda_2 > 0 \\ 1 - \exp(\frac{R_\beta^{\,2}}{2\beta^2})(1 - \exp(\frac{T^2}{2c^2})) & \text{otherwise} \end{cases} \quad (12)$$

Where $R_\beta = \lambda_1 / \lambda_2$ represents the eccentricity of a second order ellipse, c affects filter sensitivity, and $T = \sqrt{\lambda_1^{\,2} + \lambda_2^{\,2}}$.

The second energy term, E_d considers the direction of minimum principal curvature at point p and q and determines if they are in line.

$$E_d(p,q) = \frac{2}{\pi} \times \arccos \left| \frac{E_d(p) \cdot E_d(q)}{\|E_d(p)\| E_d(q)\|} \right| \quad (13)$$

The third energy term, E_e, is the image evidence energy. This examined the edges of the image using the weighted sum of the Canny edge detection filter, Laplacian of Gaussian filter, and gradient magnitude filter. It is the average of N samples taken from this edge image at radius r away from center point q perpendicular to the direction of minimum curvature.

The fourth energy term, E_s, is the Euclidean distance between p and q, represents the spatial smoothness energy. The best contour between pixels p and q is the optimal path and it is then determined by Dijkstra's algorithm [24].

III. MATERIAL

Thirty EDI OCT images from patients with diabetes (one image per eye, one eye randomly chosen per patient) were used for the evaluation of the proposed technique. These images were acquired from a study followed the tenets of the Declaration of Helsinki. All EDI OCT images were acquired using a Heidelberg Spectralis+HRA OCT device (Heidelberg Engineering, Heidelberg, Germany). The axial digital image size was 496 pixels and the scan depth was 1.9 mm. The optical resolution (in μm) was 7 axially × 14 laterally. Each choroidal EDI scan was acquired using the built-in automatic averaging and real time eye-tracking features comprised of 100 averaged scans.

The outer and inner boundaries of the choroid in each EDI OCT image were manually delineated using ImageJ (NIH, US) to compare with the method proposed in this paper. The in-house computer programs used to segment the choroidal boundaries and to evaluate the agreement of the technique was written using Matlab 2012a (The MathWorks, Inc., US) and Microsoft Visual C++ 2008 Professional Edition (Microsoft Corporation, US)

IV. RESULTS

We applied the proposed technique to all thirty images. Figure 2 illustrates an example of the segmentation results of the automated method proposed in this paper (Figure 2a) and the manual annotation by an expert (Figure 2b).

During the evaluation, it is noted that the segmentation of the choroid in each image using the in-house software is very intelligent and efficient compare to manual delineation using imageJ.

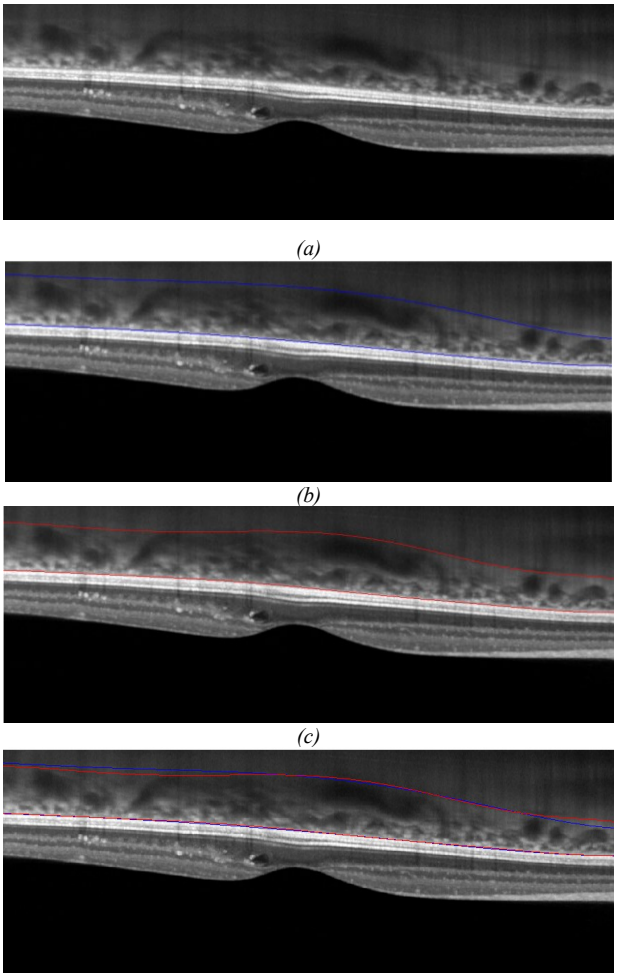

(a) *(b)* *(c)* *(d)*

Figure 2. *(a)* Original EDI OCT image of the choroid; *(b)* Automated segmentation (lines in blue) using the proposed method; *(c)* Manual annotation (lines in red); *(d)* Comparing automated segmentation result (lines in blue) with manual lineation result (lines in red).

In order to evaluate the performance of the program, the choroid area was measured by the proposed technique and manual annotation was compared at the 3 mm temporal to the fovea to 3 mm nasal to the fovea.The agreement between the proposed technique and the expert is quantitatively measured by using commonly used Dice similarity coefficient (DSC):

$$DSC = \frac{2 \times |I_a \cap I_b|}{|I_a + I_b|} \quad (14)$$

Where I_a and I_b represents the segmentation of the proposed technique and that of an expert. "$\cap$" denotes the

intersection between two segmentations. Figure 3 shows the DSC values within 30 images. The mean DSC value is 92.7% (standard deviation 3.6%) in the range of 85.5% to 98.1%.

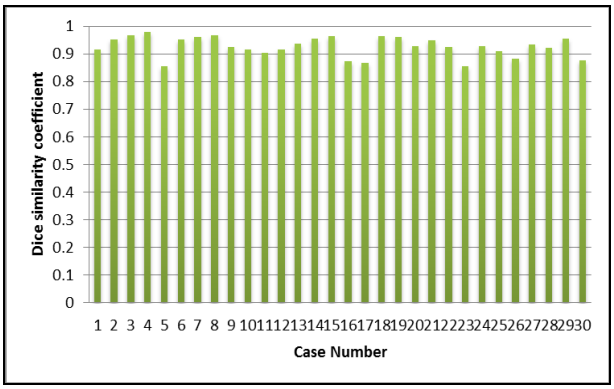

Figure 3. Dice similarity coefficient results of 30 patients

V. CONCLUSION

In this paper, a novel segmentation model is proposed for automated segmentation of the choroid in EDI OCT images. Our experimental results showed excellent agreements between the proposed technique and manual annotations by the expert. The software is easy to use and has a high efficiency compares to manual annotations. One important advantage of this technique is its real-time human interaction which intelligently guides the segmentation of the outer border which is difficult to be automatically segmented. This technique is able to segment the choroid in the EDI OCT images generated by other OCT devices .

In future work, we will further evaluate the efficiency in terms of computational time and the intra- and inter-observer variability of this choroidal image segmentation technique. Moreover, we can include other commonly used metrics for OCT image analysis, such as Hausdorff distance and mean signed (or unsigned) positioning errors, for the evaluation of the segmentation accuracy. We also plan to extend this work to segment the choroid in 3D volume scans in normal and diseased retina.

REFERENCES

[1] D. L. Nickla and J. Wallman, "The multifunctional choroid," *Prog Retin Eye Res,* vol. 29, pp. 144-68, 2010.

[2] F. V. Jonh, D. D. Andrew, M. G. Paul, and R. Fiona, *Anatomy of the eye and orbit*. Edinburgh: W.B. Saunders, 2002.

[3] C. W. Spraul, G. E. Lang, and H. E. Grossniklaus, "Morphometric analysis of the choroid, Bruch's membrane, and retinal pigment epithelium in eyes with age-related macular degeneration," *Invest Ophthalmol Vis Sci,* vol. 37, pp. 2724-35, 1996.

[4] V. Manjunath, J. Goren, J. G. Fujimoto, and J. S. Duker, "Analysis of choroidal thickness in age-related macular degeneration using spectral-domain optical coherence tomography," *Am J Ophthalmol,* vol. 152, pp. 663-8, 2011.

[5] S. W. Kim, J. Oh, S. S. Kwon, J. Yoo, and K. Huh, "Comparison of choroidal thickness among patients with healthy eyes, early age-related maculopathy, neovascular age-related macular degeneration, central serous chorioretinopathy, and polypoidal choroidal vasculopathy," *Retina,* vol. 31, pp. 1904-11, 2011.

[6] S. E. Chung, S. W. Kang, J. H. Lee, and Y. T. Kim, "Choroidal thickness in polypoidal choroidal vasculopathy and exudative age-related macular degeneration," *Ophthalmology,* vol. 118, pp. 840-5, 2011.

[7] J. R. Ehrlich, J. Peterson, G. Parlitsis, K. Y. Kay, S. Kiss, and N. M. Radcliffe, "Peripapillary choroidal thickness in glaucoma measured with optical coherence tomography," *Exp Eye Res,* vol. 92, pp. 189-94, 2011.

[8] E. A. Maul, D. S. Friedman, D. S. Chang, M. V. Boland, P. Y. Ramulu, H. D. Jampel, and H. A. Quigley, "Choroidal thickness measured by spectral domain optical coherence tomography: factors affecting thickness in glaucoma patients," *Ophthalmology,* vol. 118, pp. 1571-9, 2011.

[9] Y. T. Kim, S. W. Kang, and K. H. Bai, "Choroidal thickness in both eyes of patients with unilaterally active central serous chorioretinopathy," *Eye (Lond),* vol. 25, pp. 1635-40, 2011.

[10] I. Maruko, T. Iida, Y. Sugano, A. Ojima, and T. Sekiryu, "Subfoveal choroidal thickness in fellow eyes of patients with central serous chorioretinopathy," *Retina,* vol. 31, pp. 1603-8, 2011.

[11] M. Esmaeelpour, B. Povazay, B. Hermann, B. Hofer, V. Kajic, S. L. Hale, R. V. North, W. Drexler, and N. J. Sheen, "Mapping choroidal and retinal thickness variation in type 2 diabetes using three-dimensional 1060-nm optical coherence tomography," *Invest Ophthalmol Vis Sci,* vol. 52, pp. 5311-6, 2011.

[12] X. Ding, J. Li, J. Zeng, W. Ma, R. Liu, T. Li, S. Yu, and S. Tang, "Choroidal thickness in healthy Chinese subjects," *Invest Ophthalmol Vis Sci,* vol. 52, pp. 9555-60, 2011.

[13] S. Usui, Y. Ikuno, A. Miki, K. Matsushita, Y. Yasuno, and K. Nishida, "Evaluation of the choroidal thickness using high-penetration optical coherence tomography with long wavelength in highly myopic normal-tension glaucoma," *Am J Ophthalmol,* vol. 153, pp. 10-6 e1, 2012.

[14] Z. Hu, X. Wu, Y. Ouyang, Y. Ouyang, and S. R. Sadda, "Semi-automated Segmentation of the Choroid in Spectral-domain Optical Coherence Tomography Volume Scans," *Invest Ophthalmol Vis Sci,* 2013.

[15] L. Zhang, K. Lee, M. Niemeijer, R. F. Mullins, M. Sonka, and M. D. Abramoff, "Automated segmentation of the choroid from clinical SD-OCT," *Invest Ophthalmol Vis Sci,* vol. 53, pp. 7510-9, 2012.

[16] V. Kajic, M. Esmaeelpour, B. Povazay, D. Marshall, P. L. Rosin, and W. Drexler, "Automated choroidal segmentation of 1060 nm OCT in healthy and pathologic eyes using a statistical model," *Biomedical Optics Express,* vol. 3, pp. 86-103, 2012.

[17] K. Poon, G. Hamarneh, and R. Abugharbieh, "Live-vessel: extending livewire for simultaneous extraction of optimal medial and boundary paths in vascular images," *Med Image Comput Comput Assist Interv,* vol. 10, pp. 444-51, 2007.

[18] X. Bresson, S. Esedoglu, P. Vandergheynst, J. P. Thiran, and S. Osher, "Fast global minimization of the active Contour/Snake model," *Journal of Mathematical Imaging and Vision,* vol. 28, pp. 151-167, 2007.

[19] T. F. Chan and L. A. Vese, "Active Contours Without Edges," *IEEE Transactions on Image Processing,* vol. 10, pp. 266-277, 2001.

[20] A. Chambolle, "An algorithm for total variation minimization and applications," *Journal of Mathematical Imaging and Vision,* vol. 20, pp. 89-97, 2004.

[21] Y. Zheng and K. Chen, "A Hierarchical Algorithm for Multiphase Texture Image Segmentation," *ISRN Signal Processing,* 2012.

[22] K. Ni, B. W. Hong, S. Soatto, and T. F. Chan, "Unsupervised multiphase segmentation: a recursive approach," *Computer Vision and Image Understanding,* vol. 113, pp. 502-510, 2009.

[23] G. Mylonas, C. Ahlers, P. Malamos, I. Golbaz, G. Deak, C. Schuetze, S. Sacu, and U. Schmidt-Erfurth, "Comparison of retinal thickness measurements and segmentation performance of four different spectral and time domain OCT devices in neovascular age-related macular degeneration," *British Journal of Ophthalmology,* vol. 93, pp. 1453-1460, 2009.

[24] E. W. Dijkstra, "A note on two problems in connexion with graphs," *Numerische Mathematik,* vol. 1, pp. 269-271, 1959.